Robustness of Connected Vehicle Systems

D. Hajdu & T. Insperger*
Department of Applied Mechanics
Budapest University of Technology and Economics, Budapest, Hungary
***MTA-BME Lendület Human Balancing Research Group**
E-mail: hajdu@mm.bme.hu

J. I. Ge
Department of Computational and Mathematical Sciences
California Institute of Technology, Pasadena, CA 91125, USA

G. Orosz
Department of Mechanical Engineering
University of Michigan, Ann Arbor, MI 48109, USA

Topics/Vehicle Automation and Connection

May 14, 2018

Since a connected cruise controller utilizes motion information from multiple human-driven vehicles ahead, its performance significantly depends on human driving behavior. Therefore, robust controller designis required to maintain a desired level of performance against uncertainties in human parameters. In this paper, we apply structured singular value analysis to select robust control gains that guarantee string stability against uncertainties arising from the feedback gains and reaction time delays of the human drivers ahead. We demonstrate the results on a connected vehicle system where a connected automated vehicle follows three human-driven vehicles.

1 INTRODUCTION

In order to improve active safety, passenger comfort, and traffic efficiency, automation of passenger vehicles has become a widely studied area over the past few decades. While adaptive cruise control (ACC) was invented to alleviate human drivers from the constant burden of speed control [1], it only allows an equipped vehicle to respond to its immediate predecessor [2]. To overcome this limitation, cooperative adaptive cruise control (CACC) was proposed, which allows several automated vehicles to drive cooperatively through vehicle-to-vehicle (V2V) communication [3, 4, 5, 6]. However, to fully exploit the benefits of V2V communication, the V2V signals from nearby human-driven cars should also be utilized before automated vehicles become widespread. Therefore, connected cruise control (CCC) was proposed that allows an automated vehicle to respond to multiple human-driven vehicles ahead via ad-hoc V2V communication [7, 8, 9, 10].

Since both CACC and CCC designs rely on the dynamics of multiple preceding vehicles, parameter uncertainties among these vehicles need to be considered in order to guarantee robust performance. For CACC designs, [11, 12, 13] considered the uncertainties among an automated platoon and synthesized robust controllers using the $\mathcal{H}_\infty$ framework. Some other methods were also used in [14, 15, 16, 17] to discuss the effects of unmodeled dynamics, stochastic communication delay, and measurement noise. However, to obtain robust CCC designs, a systematic method is needed to not only consider the uncertain feedback parameters but also the reaction time delay of nearby human drivers. In this paper, we use structured singular value analysis [18, 19] to evaluate the effects of uncertain human parameters on CCC design, and demonstrate the results by ensuring robust head-to-tail string stability on a four-vehicle configuration.

2 CONNECTED VEHICLE SYSTEMS

In this section we describe the longitudinal dynamics of a connected vehicle system. We consider a heterogeneous chain of vehicles where all vehicles are equipped with V2V devices and some are capable of automated driving, as shown in Fig. 1. When an automated vehicle receives motion information broadcasted from several vehicles ahead, it may choose to use the information in its motion control (see the dashed arrows), and thus, it becomes a connected automated vehicle. Such a V2V-based controller then defines a connected vehicle system consisting of the connected automated vehicle and the preceding vehicles whose motion signals are used by the connected automated vehicle.

Inside this connected vehicle system, we denote the connected automated vehicle as vehicle 0, and the preceding vehicles as vehicles $1,\dots,n$. The longitudinal dynamics of human-driven vehicle i can be described by

$$\begin{aligned}\dot{h}_i(t) &= v_{i+1}(t) - v_i(t)\,,\\ \dot{v}_i(t) &= \alpha_i\big(V_i\big(h_i(t-\tau_i)\big) - v_i(t-\tau_i)\big)\\ &\quad + \beta_i\big(v_{i+1}(t-\tau_i) - v_i(t-\tau_i)\big),\end{aligned} \tag{1}$$

for $i=1,\dots,n$, where h_i and v_i are the headway and speed of vehicle i, α_i and β_i are the control gains and the time delay τ_i accounts for the reaction time delay of a human driver plus the actuator delay of the vehicle. Moreover, $V_i(h_i)$ is the range policy function that describes the desired velocity based on headway

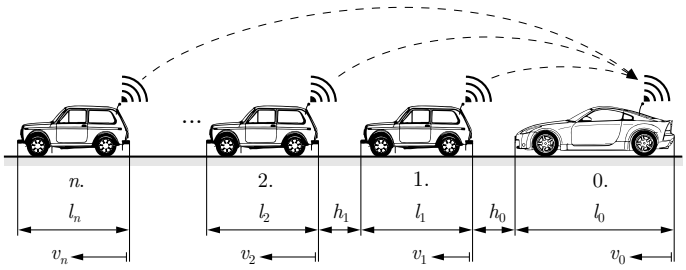

Figure 1: A connected vehicle system arising from the V2V-based controller of a connected automated vehicle.

h_i. Inspired by model (1) we design the longitudinal controller for the connected automated vehicle 0 in the form of

$$\begin{aligned}\dot{h}_0(t) &= v_1(t) - v_0(t)\,,\\ \dot{v}_0(t) &= a_{1,0}\big(V_0\big(h_0(t-\sigma_{1,0})\big) - v_0(t-\sigma_{1,0})\big)\\ &\quad + \sum_{j=1}^{n} b_{j,0}\big(v_j(t-\sigma_{j,0}) - v_0(t-\sigma_{j,0})\big), \end{aligned} \tag{2}$$

where the control gains $a_{j,0}$, $b_{j,0}$ and delay $\sigma_{j,0}$ correspond to the links between vehicle j and the connected automated vehicle 0. Note that the delay $\sigma_{j,0}$ arises from the actuators as well as from communication intermittency and possible packet losses.

The range policy function is assumed to be similar for each vehicle, i.e.,

$$V_i(h_i) = \begin{cases} 0 & \text{if} \quad h_i \le h_{\text{st},i}\,,\\ \kappa_i(h_i - h_{\text{st},i}) & \text{if} \quad h_{\text{st},i} < h_i < h_{\text{go},i}\,,\\ v_{\max} & \text{if} \quad h_i \ge h_{\text{go},i}\,, \end{cases} \tag{3}$$

where $\kappa_i = v_{\max}/(h_{\text{go},i} - h_{\text{st},i})$. That is, the desired velocity is zero for small headways ($h_i \le h_{\text{st},i}$) and equal to the speed limit $v_{\max}$ for large headways ($h_i \ge h_{\text{go},i}$). Between these, the desired velocity increases with the headway linearly, with gradient κ_i. Many other range policies may be chosen, but the qualitative dynamics remain similar if the above characteristics are kept.

Unlike many cooperative adaptive cruise control algorithms, the preceding vehicles $1,\dots,n$ in the connected vehicle system shown in Fig. 1 are not required to cooperate with the connected automated vehicle. That is, aside from broadcasting their motion information through V2V communication, no automation of these vehicles is required. Thus, the feedback gains and delay time in (1) cannot be tuned for the connected automated vehicle design. However, the connected automated vehicle 0 may fully exploit V2V signals from vehicles $1,\dots,n$ with no constraint on the connectivity topology.

We consider the stability of the connected vehicle system (1-2) around the equilibrium where the vehicles travel with the same speed $v_i(t) = v^*$ and their corresponding headways are $h_i(t) = h_i^*$ such that $V_i(h_i^*) = v^*$, $i = 0,\dots,n$. We define the perturbations about the equilibrium (h_i^*, v^*) as

$$\tilde{h}_i(t) = h_i(t) - h^*, \quad \tilde{v}_i(t) = v_i(t) - v^*\,. \tag{4}$$

Since we are interested in how speed perturbations $\tilde{v}_i$ propagate through the connected vehicle system, especially how a connected automated vehicle attenuates such perturbations, we linearize (1-2) around the equilibrium (h_i^*, v^*) and obtain

$$\begin{aligned}\dot{\tilde{h}}_0(t) &= \tilde{v}_1(t) - \tilde{v}_0(t)\,,\\ \dot{\tilde{v}}_0(t) &= a_{1,0}\big(\kappa_0\tilde{h}_0(t-\sigma_{1,0}) - \tilde{v}_0(t-\sigma_{1,0})\big)\\ &\quad + \sum_{j=1}^{n} b_{j,0}\big(\tilde{v}_j(t-\sigma_{j,0}) - \tilde{v}_0(t-\sigma_{j,0})\big), \end{aligned} \tag{5}$$

$$\begin{aligned}\dot{\tilde{h}}_i(t) &= \tilde{v}_{i+1}(t) - \tilde{v}_i(t)\,,\\ \dot{\tilde{v}}_i(t) &= \alpha_i\big(\kappa_i\tilde{h}_i(t-\tau_i) - \tilde{v}_i(t-\tau_i)\big)\\ &\quad + \beta_i\big(\tilde{v}_{i+1}(t-\tau_i) - \tilde{v}_i(t-\tau_i)\big), \end{aligned} \tag{6}$$

for $i = 1,\dots,n$.

We assume that the connected vehicle system (5-6) is plant stable, that is, when the input perturbation $\tilde{v}_{n+1}(t) \equiv 0$, the perturbations $\tilde{h}_i$, $\tilde{v}_i$ of the preceding vehicles and $\tilde{h}_0$, $\tilde{v}_0$ of the connected automated vehicle will tend to zero regardless of the initial conditions. Instead, we focus on how the connected automated vehicle responds to speed perturbations propagating through the system. When the speed fluctuation $\tilde{v}_0$ of the connected automated vehicle has smaller amplitude than the input $\tilde{v}_n$, we call the connected automated vehicle design head-to-tail string stable. That is, head-to-tail string stability allows speed perturbations to be amplified among the uncontrollable vehicles $1,\dots,n$, and we focus on how the connected automated vehicle attenuates the perturbations. Being head-to-tail string stable not only enables a connected automated vehicle to enjoy better active safety, fuel economy, and passenger comfort, it can also improve the efficiency of the traffic flow [8].

We assume zero initial conditions for (5-6) and obtain

$$\tilde{V}_0(s) = \sum_{i=1}^{n} T_{i,0}(s)\tilde{V}_i(s), \tag{7}$$

$$\tilde{V}_i(s) = T_{i+1,i}(s)\tilde{V}_{i+1}(s)\,, \tag{8}$$

where $\tilde{V}_0(s)$ and $\tilde{V}_i(s)$ denote the Laplace transform of $\tilde{v}_0(t)$ and $\tilde{v}_i(t)$, and the link transfer functions are

$$\begin{aligned} T_{1,0}(s) &= \frac{(a_{1,0}\kappa_0 + b_{1,0}s)\mathrm{e}^{-s\sigma_{1,0}}}{s^2 + a_{1,0}(\kappa_0 + s)\mathrm{e}^{-s\sigma_{1,0}} + \sum_{l=1}^{n} b_{l,0}s\mathrm{e}^{-s\sigma_{l,0}}}\,,\\ T_{i,0}(s) &= \frac{b_{i,0}s\mathrm{e}^{-s\sigma_{j,0}}}{s^2 + a_{1,0}(\kappa_0 + s)\mathrm{e}^{-s\sigma_{1,0}} + \sum_{l=1}^{n} b_{l,0}s\mathrm{e}^{-s\sigma_{l,0}}}\,,\\ T_{i+1,i}(s) &= \frac{(\alpha_i\kappa_i + \beta_i s)\mathrm{e}^{-s\tau_i}}{s^2 + (\alpha_i\kappa_i + (\alpha_i + \beta_i)s)\mathrm{e}^{-s\tau_i}}\,. \end{aligned} \tag{9}$$

for $i = 1,\dots,n$. Thus, the head-to-tail transfer function of the connected vehicle system is

$$G_{n,0}(s) = \frac{\tilde{V}_0(s)}{\tilde{V}_n(s)} = \det\left(\mathbf{T}\left(s\right)\right)\,, \tag{10}$$

where the transfer function matrix is

$$\mathbf{T}(s) = \begin{bmatrix} T_{1,0}(s) & -1 & 0 & \cdots & 0\\ T_{2,0}(s) & T_{2,1}(s) & -1 & \cdots & 0\\ \vdots & \vdots & \vdots & \ddots & \vdots\\ T_{n-1,0}(s) & T_{n-1,1}(s) & T_{n-1,2}(s) & \cdots & -1\\ T_{n,0}(s) & T_{n,1}(s) & T_{n,2}(s) & \cdots & T_{n,n-1}(s) \end{bmatrix}, \tag{11}$$

see [8] for the proof.

The criterion for head-to-tail string stability at the linear level is guaranteed if the perturbations are attenuated for any frequency, that is, if

$$\big|\det\big(\mathbf{T}(\mathrm{i}\omega)\big)\big| < 1, \quad \forall\,\omega > 0\,, \tag{12}$$

where we substituted $s = \mathrm{i}\omega$. In order to facilitate robustness analysis we rewrite (12) as

$$1 - \det\big(\mathbf{T}(\mathrm{i}\omega)\big)\delta^{\mathrm{c}} \neq 0, \quad \forall\,\omega > 0\,, \tag{13}$$

where δ^{c} is an arbitrary complex number inside the unit circle in the complex plane, that is, $\delta^{\mathrm{c}} \in \mathbb{C}$, $|\delta^{\mathrm{c}}| < 1$.

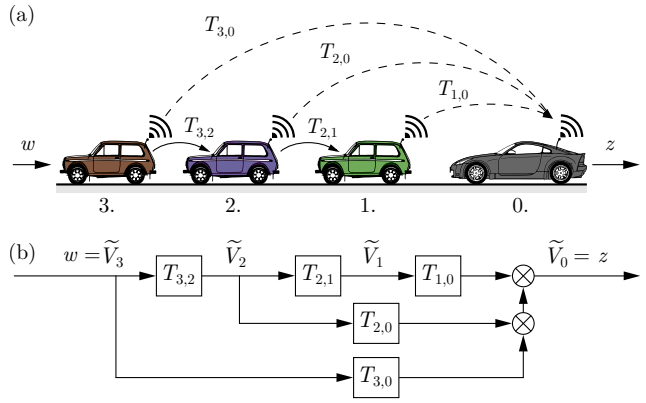

Figure 2: Example configuration: (a) Connected vehicle structure. (b) Block diagram.

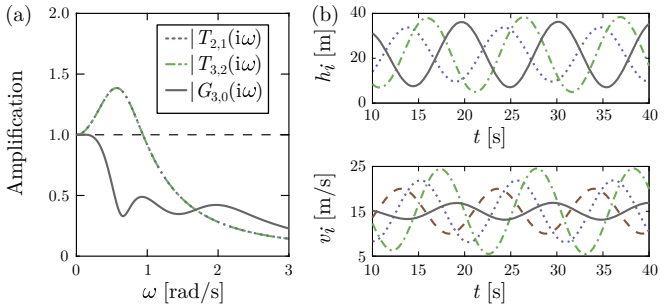

Figure 3: Example transfer functions $|T_{3,2}(\mathrm{i}\omega)|$, $|T_{2,1}(\mathrm{i}\omega)|$, $|G_{3,0}(\mathrm{i}\omega)|$ and corresponding simulations with $\omega^* = 0.6$ [rad/s].

To illustrate the head-to-tail string stability, here we consider a connected automated vehicle using motion information from three vehicles ahead ($n = 3$), as shown in Fig. 2(a). The transfer function matrix for this connected vehicle system is

$$\mathbf{T}(s) = \begin{bmatrix} T_{1,0}(s) & -1 & 0 \\ T_{2,0}(s) & T_{2,1}(s) & -1 \\ T_{3,0}(s) & 0 & T_{3,2}(s) \end{bmatrix}, \tag{14}$$

where the elements $T_{1,0}(s), T_{2,0}(s), T_{3,0}(s), T_{2,1}(s)$ and $T_{3,2}(s)$ are given by (9), while (10) gives the head-to-tail transfer function

$$G_{3,0}(s) = T_{3,2}(s)\big(T_{2,1}(s)T_{1,0}(s) + T_{2,0}(s)\big) + T_{3,0}(s). \tag{15}$$

The flow of information is illustrated by a block diagram in Fig. 2(b). We consider the case when the preceding vehicles $i = 1, 2$ have parameters $\alpha_i = 0.2$ [1/s], $\beta_i = 0.4$ [1/s], $\kappa_i = 0.9$ [1/s], $\tau_i = 0.9$ [s], and the design parameters are $a_{1,0} = 0.4$ [1/s], $b_{1,0} = 0.2$ [1/s], $b_{2,0} = 0.4$ [1/s], $b_{3,0} = 0.4$ [1/s], $\kappa_0 = 0.9$ [1/s], and $\sigma_{1,0} = \sigma_{2,0} = \sigma_{3,0} = \sigma = 0.6$ [s] for the connected automated vehicle.

In Fig. 3(a) we plot the head-to-tail transfer function $|G_{3,0}(\mathrm{i}\omega)|$ of the connected automated vehicle (solid gray curve) and the link transfer function $|T_{3,2}(\mathrm{i}\omega)|$ that describes how vehicle 2 responds to the motion of vehicle 3 (dotted purple curve). Here this is equal to $|T_{2,1}(\mathrm{i}\omega)|$ as vehicles 2 and 1 have the same parameters. While the magnitude of the head-to-tail transfer function stays below 1, the link transfer functions of vehicles 2 and 1 reach beyond 1 for low frequencies. This indicates that speed perturbations at low frequency are amplified by vehicles 2 and 1 but eventually are suppressed by the connected automated vehicle. This observation is supported by a simulation shown in Fig. 3(b), where the speed input $v_3(t) = 15 + 5\sin(\omega^* t)$ is applied with $\omega^* = 0.6$ [rad/s]. The color code corresponds to the vehicle colors in Fig. 2(a).

Note that the results shown in Fig. 3 strongly depend on the parameters of the preceding vehicles. The same control parameters used in Fig. 3 may behave poorly with a different set of parameters κ_i, α_i, β_i and τ_i. In the forthcoming sections, we will assume additive perturbation in these parameters denoted by $\tilde{\kappa}_i$, $\tilde{\alpha}_i$, $\tilde{\beta}_i$ and $\tilde{\tau}_i$, and apply robust control design to ensure head-to-tail string stability under these parameter changes.

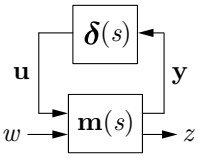

Figure 4: $\mathbf{m} - \boldsymbol{\delta}$ uncertain interconnection structure.

3 ROBUST STRING STABILITY

Since a connected automated vehicle may not know the dynamics of the preceding vehicles $1, \ldots, n$ accurately, the V2V-based controller should be robust against their parameter uncertainties beside from the model uncertainties of the connected automated vehicle itself. Based on the theory of robust control, we represent the system uncertainty in the $\mathbf{m} - \boldsymbol{\delta}$ uncertain interconnection structure, as shown in Fig. 4 [18, 19]. We present the formulation of interconnected model for the two-vehicle configuration briefly, then extend the results for connected vehicle systems. Examples are given on a four-vehicle model, which can be easily generalized further.

3.1 Two-vehicle configuration

To introduce the robust string stability, we start with the simplest case where vehicle i only uses information from the vehicle immediately ahead, see Fig. 5(a). In this case the input of the nominal system is $\tilde{v}_{i+1}(t)$ while the output is $\tilde{v}_i(t)$, and the link transfer function is given by

$$T_{i+1,i}(s) = \frac{(\alpha\kappa + \beta s)\mathrm{e}^{-s\tau}}{s^2 + (\alpha\kappa + (\alpha + \beta)s)\mathrm{e}^{-s\tau}}, \tag{16}$$

where we dropped the subscripts of the parameters κ, α, β, and τ; see (9).

While the additive uncertainties $\tilde{\alpha}$, $\tilde{\beta}$, and $\tilde{\kappa}$ result in additive uncertainty terms, an additive delay uncertainty $\tilde{\tau}$ results in a multiplicative exponential term $\mathrm{e}^{-s\tilde{\tau}}$ in (16), that is,

$$\begin{aligned} &T_{i+1,i}(s) + \tilde{T}_{i+1,i}(s) \\ &= \frac{\big((\kappa + \tilde{\kappa})(\alpha + \tilde{\alpha}) + (\beta + \tilde{\beta})s\big)\mathrm{e}^{-s(\tau+\tilde{\tau})}}{s^2 + \big((\kappa + \tilde{\kappa})(\alpha + \tilde{\alpha}) + (\alpha + \tilde{\alpha} + \beta + \tilde{\beta})s\big)\mathrm{e}^{-s(\tau+\tilde{\tau})}}, \end{aligned} \tag{17}$$

where $\tilde{T}_{i+1,i}(s)$ represents the uncertainty. In order to formulate the uncertainties in a way that can be represented by the $\mathbf{m} - \boldsymbol{\delta}$ interconnection structure, we use the approximation

$$\mathrm{e}^{-s(\tau+\tilde{\tau})} \approx \mathrm{e}^{-s\tau}\big(1 + \tilde{\vartheta}(s)\big), \tag{18}$$

where

$$\tilde{\vartheta}(s) = \frac{\tilde{\tau}s}{1 + \tilde{\tau}s/3.456}\epsilon, \quad \epsilon \in \mathbb{C},\ |\epsilon| < 1 \tag{19}$$

estimates the uncertainty, see [20]. By taking into account the uncertain parameters, the block diagram in Fig. 5(b) can be drawn. This illustrates how uncertainties affect the system and allows one to construct the $\mathbf{m} - \boldsymbol{\delta}$ structure by solving a number of algebraic equations.

Based on Fig. 5(b), one can derive the linear system of equations in the form

$$\begin{bmatrix} \mathbf{y} \\ z \end{bmatrix} = \mathbf{m}(s) \begin{bmatrix} \mathbf{u} \\ w \end{bmatrix}, \tag{20}$$

$$\mathbf{u} = \boldsymbol{\delta}(s)\mathbf{y}, \tag{21}$$

$$\mathbf{m}(s)=\frac{1}{D(s)}\left[\begin{array}{cccc|c} -\alpha \mathrm{e}^{-s\tau} & -\mathrm{e}^{-s\tau} & -\mathrm{e}^{-s\tau} & -2 & s+\alpha \mathrm{e}^{-s\tau} \\ s^2+\beta s \mathrm{e}^{-s\tau} & -(\kappa+s)\mathrm{e}^{-s\tau} & -(\kappa+s)\mathrm{e}^{-s\tau} & 2(\kappa+s) & \kappa s-\beta s \mathrm{e}^{-s\tau} \\ -\alpha s \mathrm{e}^{-s\tau} & -s\mathrm{e}^{-s\tau} & -s\mathrm{e}^{-s\tau} & 2s & s^2+\alpha s \mathrm{e}^{-s\tau} \\ \alpha s^3 \mathrm{e}^{-s\tau} & s^3\mathrm{e}^{-s\tau} & s^3\mathrm{e}^{-s\tau} & -s^3+s\big(\kappa\alpha+s(\alpha+\beta)\big)\mathrm{e}^{-s\tau} & (\kappa\alpha s^2+\beta s^3)\mathrm{e}^{-s\tau} \\ \hline \alpha s \mathrm{e}^{-s\tau} & s\mathrm{e}^{-s\tau} & s\mathrm{e}^{-s\tau} & -2s & (\kappa\alpha+\beta s)\mathrm{e}^{-s\tau} \end{array}\right], \tag{23}$$

$$D(s)=s^2+\big(\kappa\alpha+s(\alpha+\beta)\big)\mathrm{e}^{-s\tau}, \tag{24}$$

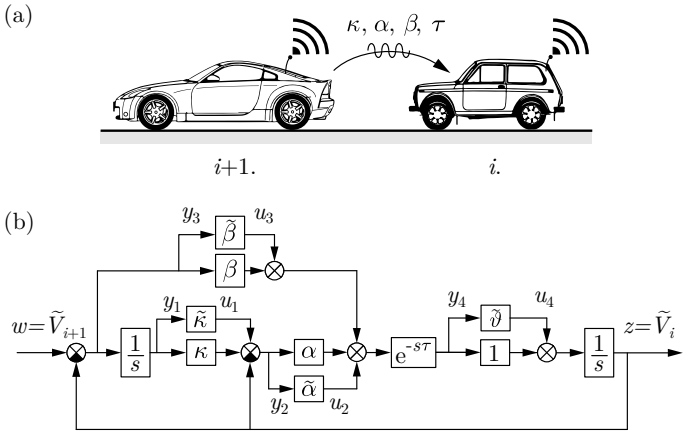

Figure 5: Two-vehicle configuration: (a) Connected vehicle system. (b) Block diagram of the uncertain transfer function.

where $\mathbf{m}(s)$ is partitioned as

$$\mathbf{m}(s)=\left[\begin{array}{c|c} \mathbf{m}_{1,1}(s) & \mathbf{m}_{1,2}(s) \\ \hline \mathbf{m}_{2,1}(s) & m_{2,2}(s) \end{array}\right]. \tag{22}$$

More precisely, the generalized transfer function matrix $\mathbf{m}(s)$ can be given by (23-24), and the matrix of uncertainties are collected in

$$\boldsymbol{\delta}(s)=\mathrm{diag}\left[\tilde{\kappa},\tilde{\alpha},\tilde{\beta},\tilde{\vartheta}(s)\right]. \tag{25}$$

The transfer function between the input $w=\tilde{V}_{i+1}(s)$ and output $z=\tilde{V}_i(s)$ with uncertainties can be written in terms of upper linear fractional transformations (LFT), such that

$$\begin{aligned}\mathcal{F}_{\mathrm{u}}\big(\mathbf{m}(s),\boldsymbol{\delta}(s)\big)&=T_{i+1,i}(s)+\tilde{T}_{i+1,i}(s)\\ &=\underbrace{m_{2,2}(s)}_{T_{i+1,i}(s)}+\underbrace{\mathbf{m}_{2,1}(s)\boldsymbol{\delta}(s)\big(\mathbf{I}-\mathbf{m}_{1,1}(s)\boldsymbol{\delta}(s)\big)^{-1}\mathbf{m}_{1,2}(s)}_{\tilde{T}_{i+1,i}(s)}\\ &=\frac{\big((\kappa+\tilde{\kappa})(\alpha+\tilde{\alpha})+(\beta+\tilde{\beta})s\big)\mathrm{e}^{-s\tau}(1+\tilde{\vartheta}(s))}{s^2+\big((\kappa+\tilde{\kappa})(\alpha+\tilde{\alpha})+(\alpha+\tilde{\alpha}+\beta+\tilde{\beta})s\big)\mathrm{e}^{-s\tau}(1+\tilde{\vartheta}(s))}\end{aligned} \tag{26}$$

under the condition $\det(\mathbf{I}-\mathbf{m}_{1,1}(s)\boldsymbol{\delta}(s))\neq 0$.

Note that the elements of (25) are not normalized and some of them might be complex, while others are real parametric uncertainties. Therefore we introduce the weight matrix $\mathbf{r}(s)$ in the form

$$\mathbf{r}(s)=\mathrm{diag}\left[\rho_1,\rho_2,\rho_3,\rho_4(s)\right], \tag{27}$$

where $\tilde{\kappa}=\rho_1\delta_1^{\mathrm{r}}$, $\tilde{\alpha}=\rho_2\delta_2^{\mathrm{r}}$, $\tilde{\beta}=\rho_3\delta_3^{\mathrm{r}}$, $\tilde{\vartheta}(s)=\rho_4(s)\delta_4^{\mathrm{c}}$, for $|\delta_k^{\mathrm{r}}|<1$, $\delta_k^{\mathrm{r}}\in\mathbb{R}$, $k=1,2,3$, and $|\delta_4^{\mathrm{c}}|<1$, $\delta_4^{\mathrm{c}}\in\mathbb{C}$. Thus, the normalized perturbation matrix $\hat{\boldsymbol{\delta}}$ reads

$$\hat{\boldsymbol{\delta}}=\mathrm{diag}\left[\delta_1^{\mathrm{r}},\delta_2^{\mathrm{r}},\delta_3^{\mathrm{r}},\delta_4^{\mathrm{c}}\right], \tag{28}$$

and

$$\hat{\mathbf{m}}(\omega)=\begin{bmatrix}\mathbf{m}_{1,1}(s)\mathbf{r}(s) & \mathbf{m}_{1,2}(s)\\ \mathbf{m}_{2,1}(s)\mathbf{r}(s) & m_{2,2}(s)\end{bmatrix}, \tag{29}$$

such that $\mathcal{F}_{\mathrm{u}}\big(\mathbf{m}(s),\boldsymbol{\delta}(s)\big)=\mathcal{F}_{\mathrm{u}}\big(\hat{\mathbf{m}}(s),\hat{\boldsymbol{\delta}}(s)\big)$.

In this paper we are interested in the robust stability analysis of connected vehicle systems, therefore we do not go further with the robust analysis of the two-vehicle configuration. Instead, we apply these results when building larger systems. In particular, the $\mathbf{m}-\boldsymbol{\delta}$ model is used to construct the $\mathbf{M}-\boldsymbol{\Delta}$ model for larger systems and investigate the robust string stability of the head-to-tail transfer function afterwards.

3.2 Four-vehicle system

To demonstrate that the framework presented above can be extended for large connected vehicles networks, we consider the four-vehicle scenario in Fig 6(a), where a connected automated vehicle utilizes V2V signals from three human-driven vehicles ahead, cf. Fig. 2(a). The corresponding block diagram with uncertainties is presented in Fig. 6(b), which is the extension of Fig. 2(b). While the nominal transfer function matrix is given in (14), we assume each parameter for vehicles 2 and 1 have certain levels of uncertainty and compute the robust string stable regions in the parameter space $(a_{1,0},b_{1,0},b_{2,0},b_{3,0})$.

Similarly to the two-vehicle configuration, we formulate the $\mathbf{M}-\boldsymbol{\Delta}$ uncertain interconnection structure for the connected vehicle system as

$$\begin{bmatrix}\mathbf{y}_1\\ \mathbf{y}_2\\ z\end{bmatrix}=\mathbf{M}(s)\begin{bmatrix}\mathbf{u}_1\\ \mathbf{u}_2\\ w\end{bmatrix},\quad \begin{bmatrix}\mathbf{u}_1\\ \mathbf{u}_2\end{bmatrix}=\boldsymbol{\Delta}(s)\begin{bmatrix}\mathbf{y}_1\\ \mathbf{y}_2\end{bmatrix}, \tag{30}$$

where $\mathbf{M}(s)$ and $\boldsymbol{\Delta}(s)$ is built up from $\mathbf{m}(s)$ and $\boldsymbol{\delta}(s)$. Figure 6(b) is a graphical representation of the uncertain interconnection structure and it results in

$$\mathbf{M}(s)=\left[\begin{array}{cc|c} \mathbf{m}_{1,1}^{(1)} & \mathbf{m}_{1,2}^{(1)}\mathbf{m}_{2,1}^{(2)} & \mathbf{m}_{1,2}^{(1)}T_{3,2} \\ \mathbf{0} & \mathbf{m}_{1,1}^{(2)} & \mathbf{m}_{1,2}^{(2)} \\ \hline \mathbf{m}_{2,1}^{(1)}T_{1,0} & \mathbf{m}_{2,1}^{(2)}(T_{2,0}+T_{1,0}T_{2,1}) & G_{3,0} \end{array}\right], \tag{31}$$

where $\mathbf{m}^{(1)}$ and $\mathbf{m}^{(2)}$ represent the uncertain interconnection matrices of vehicles 1 and 2, see (22) and Fig. 6(b). The dependence on s is not spelled out for conciseness in (31). The uncertainty matrix is written as

$$\boldsymbol{\Delta}(s)=\begin{bmatrix}\boldsymbol{\delta}^{(1)}(s) & \mathbf{0}\\ \mathbf{0} & \boldsymbol{\delta}^{(2)}(s)\end{bmatrix}, \tag{32}$$

where $\boldsymbol{\delta}^{(1)}(s)$ and $\boldsymbol{\delta}^{(2)}(s)$ are uncertainties of vehicles 1 and 2, respectively, as introduced in (25). Similarly, the weight matrix reads

$$\mathbf{R}(s)=\begin{bmatrix}\mathbf{r}^{(1)}(s) & \mathbf{0}\\ \mathbf{0} & \mathbf{r}^{(2)}(s)\end{bmatrix}, \tag{33}$$

where $\mathbf{r}^{(1)}(s)$ and $\mathbf{r}^{(2)}(s)$ represent the weights of uncertainties of vehicles 1 and 2 according to (27).

The perturbed transfer function between $w=\tilde{V}_3(s)$ and $z=\tilde{V}_0(s)$ can be expressed by upper linear fractional transfor-

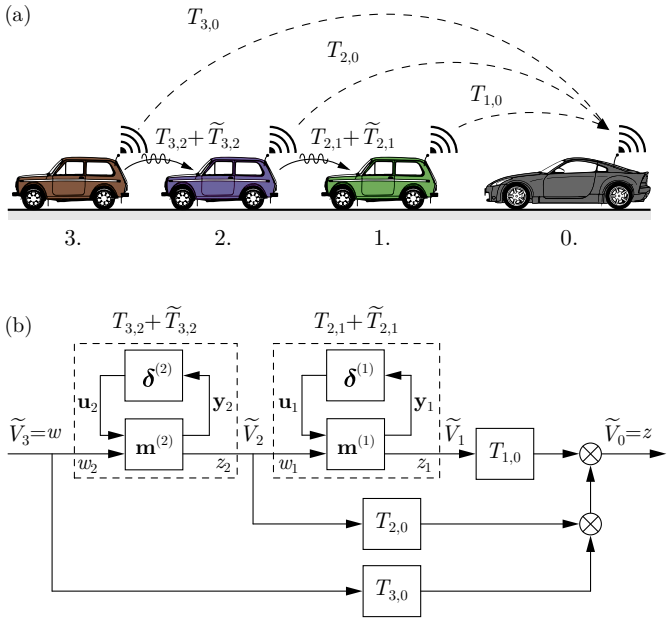

Figure 6: Four-vehicle configuration with uncertainties: (a) Connectivity topology. (b) Block diagram.

mation

$$\mathcal{F}_{\mathrm{u}}\big(\mathbf{M}(s),\boldsymbol{\Delta}(s)\big) = M_{2,2}(s)+\mathbf{M}_{2,1}(s)\boldsymbol{\Delta}(s)\big(\mathbf{I}-\mathbf{M}_{1,1}(s)\boldsymbol{\Delta}(s)\big)^{-1}\mathbf{M}_{1,2}(s), \tag{34}$$

under the condition

$$\det\big(\mathbf{I}-\mathbf{M}_{1,1}(s)\boldsymbol{\Delta}(s)\big)\neq 0\,, \tag{35}$$

which is related to the plant stability boundaries under parameter uncertainty.

Recall the string stability criterion (13), similarly, the perturbed transfer function (34), needs to satisfy

$$1-\mathcal{F}_{\mathrm{u}}\big(\mathbf{M}(\mathrm{i}\omega),\boldsymbol{\Delta}(\mathrm{i}\omega)\big)\delta_9^{\mathrm{c}}\neq,0\,,\quad \forall\,\omega>0 \tag{36}$$

and for any complex number within the unit circle, that is, $\delta_9^{\mathrm{c}}\in\mathbb{C}$, $|\delta_9^{\mathrm{c}}|<1$. Using the Schur formula (see [21]), we rewrite (35) and (36) for $s=\mathrm{i}\omega$ as

$$\det\left(\begin{bmatrix}\mathbf{I} & \mathbf{0}\\ \mathbf{0} & 1\end{bmatrix}-\begin{bmatrix}\mathbf{M}_{1,1}(\mathrm{i}\omega) & \mathbf{M}_{1,2}(\mathrm{i}\omega)\\ \mathbf{M}_{2,1}(\mathrm{i}\omega) & M_{2,2}(\mathrm{i}\omega)\end{bmatrix}\begin{bmatrix}\boldsymbol{\Delta}(\mathrm{i}\omega) & \mathbf{0}\\ \mathbf{0} & \delta_9^{\mathrm{c}}\end{bmatrix}\right)\neq 0\,. \tag{37}$$

This can be rewritten in the compact form

$$\det\big(\mathbf{I}-\hat{\mathbf{M}}(\mathrm{i}\omega)\hat{\boldsymbol{\Delta}}\big)\neq 0\,, \tag{38}$$

where

$$\hat{\mathbf{M}}(\mathrm{i}\omega)=\begin{bmatrix}\mathbf{M}_{1,1}(\mathrm{i}\omega)\mathbf{R}(\mathrm{i}\omega) & \mathbf{M}_{1,2}(\mathrm{i}\omega)\\ \mathbf{M}_{2,1}(\mathrm{i}\omega)\mathbf{R}(\mathrm{i}\omega) & M_{2,2}(\mathrm{i}\omega)\end{bmatrix}, \tag{39}$$

$$\hat{\boldsymbol{\Delta}}=\mathrm{diag}\big[\underbrace{\delta_1^{\mathrm{r}},\delta_2^{\mathrm{r}},\delta_3^{\mathrm{r}},\delta_4^{\mathrm{c}}}_{\text{vehicle 1}},\underbrace{\delta_5^{\mathrm{r}},\delta_6^{\mathrm{r}},\delta_7^{\mathrm{r}},\delta_8^{\mathrm{c}}}_{\text{vehicle 2}},\delta_9^{\mathrm{c}}\big], \tag{40}$$

and δ_9^{c} is required to fulfill robust string stability.

In order to quantify the robustness of the system, we use the structured singular value analysis introduced by [18]. We define the μ-value of $\hat{\mathbf{M}}(\mathrm{i}\omega)$ as the inverse of the smallest $\bar{\sigma}(\hat{\boldsymbol{\Delta}})$ when (38) fails at frequency ω, i.e.,

$$\mu(\omega)=\left(\min_{\hat{\boldsymbol{\Delta}}}\big\{\bar{\sigma}(\hat{\boldsymbol{\Delta}}):\det\big(\mathbf{I}-\hat{\mathbf{M}}(\mathrm{i}\omega)\hat{\boldsymbol{\Delta}}\big)=0\big\}\right)^{-1}, \tag{41}$$

where $\bar{\sigma}(\hat{\boldsymbol{\Delta}})$ denotes the largest singular value of $\hat{\boldsymbol{\Delta}}$. As $\mu(\omega)$ increases, a smaller perturbation value in $\hat{\boldsymbol{\Delta}}$ may lead to a singular $\big(\mathbf{I}-\hat{\mathbf{M}}(\mathrm{i}\omega)\hat{\boldsymbol{\Delta}}\big)$ and results in string instability. When singularity holds for arbitrarily small perturbations, then $\mu(\omega)\to\infty$ and robustness cannot be guaranteed. On the other hand, if $\det\big(\mathbf{I}-\hat{\mathbf{M}}(\mathrm{i}\omega)\hat{\boldsymbol{\Delta}}\big)\neq 0$ for any perturbation $\hat{\boldsymbol{\Delta}}$, then $\mu(\omega)=0$ and the system is robust. Therefore, the condition for robust string stability against bounded parameter variation is

$$\mu(\omega)<1,\quad \forall\,\omega>0\,, \tag{42}$$

otherwise there exists a perturbation matrix $\hat{\boldsymbol{\Delta}}$, $\bar{\sigma}(\hat{\boldsymbol{\Delta}})<1$ such that $\det\big(\mathbf{I}-\hat{\mathbf{M}}(\mathrm{i}\omega)\hat{\boldsymbol{\Delta}}\big)=0$. If $\mu(\omega)$ goes above 1, the system can lose string stability around that frequency for certain parameters within that perturbation level. If $\mu(\omega)$ remains below 1, then robustness is guaranteed for that perturbation level.

The definition of μ according to (41) does not yield directly any tractable way to compute it, since the optimization problem is not convex in general, therefore multiple local extrema might exist [22]. Instead, we are interested in computing upper and/or lower bounds, for which several alternative formulations have been developed, see [18, 22, 23, 24]. In this paper, we use the `mussv` function in MATLAB μ-Analysis and Synthesis Toolbox [25], which implements these algorithms, and we only focus on the results, not on the numerical issues.

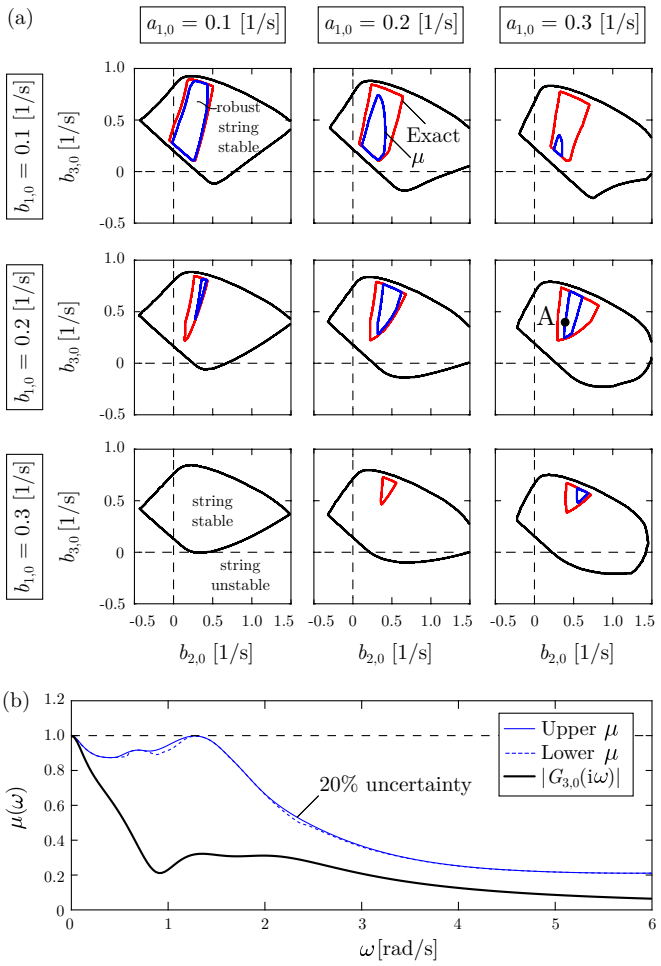

Figure 7: Four-vehicle configuration: (a) Robust stability charts in the $(b_{2,0},b_{3,0})$ plane for different values of $a_{1,0}$ and $b_{1,0}$. The black curves indicate the nominal string stability boundaries, red curves indicate the exact robust boundaries for 20% parameter uncertainty obtained from parameter sweeping, and blue curves indicate the robust boundaries obtained from μ analysis. (b) $\mu(\omega)$-curves (blue) and the nominal head-to-tail transfer function at parameter point A $(a_{1,0},b_{1,0},b_{2,0},b_{3,0})=(0.3,0.2,0.4,0.4)$ [1/s].

The results are presented in Fig. 7, where we assumed that each parameter of each uncertain vehicle is perturbed by the same percentage of their nominal value, i.e. α_i, β_i, κ_i and τ_i have identical relative uncertainties. The nominal human driver parameters are $\kappa_i = 0.8$ [1/s], $\alpha_i = 0.25$ [1/s], $\beta_i = 0.5$ [1/s] and $\tau_i = 0.8$ [s] (same for both vehicles for simplicity, $i = 1, 2$), while the fixed parameters of the connected automated vehicle are $\kappa_0 = 0.6$ [1/s] and $\sigma = \sigma_{1,0} = \sigma_{2,0} = \sigma_{3,0} = 0.6$ [s]. Fig 7(a) shows how the uncertain parameters affect the robust stable domain of control parameters $(a_{1,0}, b_{1,0}, b_{2,0}, b_{3,0})$. While the nominal system (black curve) provides a relatively large string stable domain, having 20% relative uncertainty in the human parameters significantly reduces it (blue curve). In order to quantify the conservatism, the exact robust string stability boundaries are calculated by parameter sweeping (red curves). While approximation of delay uncertainty results in a conservative approximation making the blue and red curves differ, the robust domain is still captured despite the approximation.

The $\mu(\omega)$-curves are presented in Fig. 7(b) corresponding to parameter point A $(a_{1,0}, b_{1,0}, b_{2,0}, b_{3,0}) = (0.3, 0.2, 0.4, 0.4)$ [1/s], with uncertainty level 20%. The black curve indicates the absolute value of the nominal head-to-tail transfer function $|G_{3,0}(\mathrm{i}\omega)|$, while solid and dashed blue curves correspond to the upper and lower bounds of the exact $\mu(\omega)$, respectively. Since point A in Fig. 7(a) is almost at the boundary (blue curve), the $\mu(\omega)$-curve almost reaches 1 at about $\omega = 1.3$ [rad/s].

4 CONCLUSION

We applied the structured singular value analysis to investigate the influences of uncertain human driver parameters on the head-to-tail string stability of connected cruise controllers. The method was applied in a four-vehicle configuration where the robustness results were used to design connected automated vehicles that could reject traffic perturbations well despite uncertain human gains and reaction time delay.

ACKNOWLEDGMENT

This work is supported by the ÚNKP-17-3-I. New National Excellence Program of the Ministry of Human Capacities.

REFERENCES

[1] P. I. Labuhn and W. J. Chundrlik. *Adaptive cruise control*. US Patent 5,454,442. 1995.

[2] P. A. Barber et al. *Adaptive cruise control system and methodology, including control of inter-vehicle spacing*. EP Patent 1,008,482. 2009.

[3] V. Milanes et al. "Cooperative maneuvering in close environments among cybercars and dual-mode cars". In: *IEEE Transactions on Intelligent Transportation Systems* 12.1 (2011), pp. 15–24.

[4] M. Wang et al. "Rolling horizon control framework for driver assistance systems. Part II: Cooperative sensing and cooperative control". In: *Transportation Research Part C* 40 (2014), pp. 290–311.

[5] J. Ploeg, N. van de Wouw, and H. Nijmeijer. "$\mathcal{L}_\mathrm{p}$ string stability of cascaded systems: application to vehicle platooning". In: *IEEE Transactions on Control Systems Technology* 22.2 (2014), pp. 786–793.

[6] V. Milanes and S. E. Shladover. "Modeling cooperative and autonomous adaptive cruise control dynamic responses using experimental data". In: *Transportation Research Part C* 48 (2014), pp. 285–300.

[7] G. Orosz. "Connected cruise control: modeling, delay effects, and nonlinear behaviour". In: *Vehicle System Dynamics* 54.8 (2016), pp. 1147–1176.

[8] L. Zhang and G. Orosz. "Motif-based analysis of connected vehicle systems: delay effects and stability". In: *IEEE Transactions on Intelligent Transportation Systems* 17.6 (2016), pp. 1638–1651.

[9] J. I. Ge and G. Orosz. "Dynamics of connected vehicle systems with delayed acceleration feedback". In: *Transportation Research Part C* 46 (2014), pp. 46–64.

[10] S. S. Avedisov and G. Orosz. "Analysis of connected vehicle networks using network-based perturbation techniques". In: *Nonlinear Dynamics* 89.3 (2017), pp. 1651–1672.

[11] F. Gao et al. "Robust control of heterogeneous vehicular platoon with uncertain dynamics and communication delay". In: *IET Intelligent Transport Systems* 10.7 (2016), pp. 503–513.

[12] S. E. Li et al. "Robust longitudinal control of multi-vehicle systems – A distributed H-infinity method". In: *IEEE Transactions on Intelligent Transportation Systems* PP.99 (2017), pp. 1–10.

[13] Y. Zheng et al. "Platooning of connected vehicles with undirected topologies: robustness analysis and distributed H-infinity controller synthesis". In: *IEEE Transactions on Intelligent Transportation Systems* 19.15 (2018), pp. 1–12.

[14] L. Zhang, J. Sun, and G. Orosz. "Hierarchical design of connected cruise control in the presence of information delays and uncertain vehicle dynamics". In: *IEEE Transactions on Control Systems Technology* 26.1 (2018), pp. 139–150.

[15] M. di Bernardo, A. Salvi, and S. Santini. "Distributed consensus strategy for platooning of vehicles in the presence of time varying heterogeneous communication delays". In: *IEEE Transaction on Intelligent Transportation Systems* 16.1 (2015), pp. 102–112.

[16] W. B. Qin and G. Orosz. "Scalable stability analysis on large connected vehicle systems subject to stochastic communication delays". In: *Transportation Research Part C* 83 (2017), pp. 39–60.

[17] Y. Zhou et al. "Rolling horizon stochastic optimal control strategy for ACC and CACC under uncertainty". In: *Transportation Research Part C* 83 (2017), pp. 61–76.

[18] J. C. Doyle. "Analysis of feedback systems with structured uncertainties". In: *IEE Proceedings D – Control Theory and Applications* 129.6 (1982), pp. 242–250.

[19] K. Zhou and J.C. Doyle. *Essentials of Robust Control*. Prentice Hall Modular Series F. Prentice Hall, 1998.

[20] Z.-Q. Wang, P. Lundström, and S. Skogestad. "Representation of uncertain time delays in the H_∞ framework". In: *International Journal of Control* 59.3 (1994), pp. 627–638.

[21] C. Scherer. *Theory of Robust Control*. TU Delft, 2001.

[22] P. M. Young, M. P. Newlin, and J. C. Doyle. "μ Analysis with real parametric uncertainty". In: *30th IEEE Conference on Decision and Control*. 1991, pp. 1251–1256.

[23] A. Packard and J. C. Doyle. "The complex structured singular value". In: *Automatica* 29.1 (1993), pp. 71–109.

[24] M. K. H. Fan, A. L. Tits, and J. C. Doyle. "Robustness in the presence of mixed parametric uncertainty and unmodeled dynamics". In: *IEEE Transactions on Automatic Control* 36.1 (1991), pp. 25–38.

[25] G. Balas et al. *μ-Analysis and Synthesis Toolbox for Use with Matlab User's Guide*. The MathWorks Inc, 1993.